CDK12 regulates angiogenesis of advanced prostate cancer by IGFBP3

KUN ZHONG[1,2*], WENWU LUO[2*], NAN LI[3], XIN TAN[1], YUQING LI[1], SHIYUAN YIN[1], YUHANG HUANG[1], LINNA FANG[1], WEI MA[1], YONGPING CAI[1,2] and YU YIN[2]

[1]Department of Pathology, Anhui Medical University, Hefei, Anhui 230032; Departments of [2]Pathology and [3]Nephrology, The First Affiliated Hospital of Anhui Medical University, Hefei, Anhui 230022, P.R. China

Received June 10, 2023; Accepted November 16, 2023

DOI: 10.3892/ijo.2024.5608

Abstract. Prostate cancer (PCa) is a prevalent malignancy among men, with a majority of patients presenting with distant metastases at the time of initial diagnosis. These patients are at a heightened risk of developing more aggressive castration-resistant PCa following androgen deprivation therapy, which poses a greater challenge for treatment. Notably, the inhibition of tumor angiogenesis should not be considered an ineffective treatment strategy. The regulatory role of CDK12 in transcriptional and post-transcriptional processes is essential for the proper functioning of various cellular processes. In the present study, the expression of CDK12 was first knocked down in cells using CRISPR or siRNA technology. Subsequently, RNA-seq analysis, co-immunoprecipitation, western blotting, reverse transcription-quantitative polymerase chain reaction and the LinkedOmics database were employed to reveal that CDK12 inhibits insulin like growth factor binding protein 3 (IGFBP3). Western blot analysis also demonstrated that CDK12 promoted VEGFA expression by inhibiting IGFBP3, which involves the Akt signaling pathway. Then, CDK12 was found to promote PCa cell proliferation, cell migration and angiogenesis by inhibiting IGFBP3 through cell proliferation assays, cell migration assays and tube formation assays, respectively. Finally, animal experiments were performed for *in vivo* validation. It was concluded that CDK12 promoted PCa and its angiogenesis by inhibiting IGFBP3.

Correspondence to: Professor Yu Yin, Department of Pathology, The First Affiliated Hospital of Anhui Medical University, 218 Jixi Road, Hefei, Anhui 230022, P.R. China
E-mail: yinyu@ahmu.edu.cn

Professor Yongping Cai, Department of Pathology, Anhui Medical University, 81 Meishan Road, Hefei, Anhui 230032, P.R. China
E-mail: caiyongping@ahmu.edu.cn

*Contributed equally

Key words: prostate cancer, CDK12, insulin like growth factor binding protein 3, VEGF, angiogenesis

Introduction

Prostate cancer (PCa), which usually occurs in middle-aged and older men, is the top hereditary cancer type of all major cancers and is also the most common non-skin cancer in men worldwide. Despite new advances in diagnosis and treatment of PCa, this disease remains a major medical problem in men due to the overtreatment of inherently benign disease and the undertreatment of metastatic PCa (1-3). Numerous patients with PCa are at an advanced stage or have metastases at the time of diagnosis (4). In patients with distant metastases, the 5-year relative survival rate decreases from 80% in patients with no metastases to 30% (5).

Early stages of PCa are known as androgen-dependent PCa and almost all patients who receive androgen deprivation therapy (ADT) will progress to castration-resistant PCa (CRPC) (6,7). CRPC is prone to distant metastasis and is more aggressive, making it very difficult to treat (7). PCa treated with ADT is also susceptible to neuroendocrine transformation and even evolution to neuroendocrine PCa (NEPC) (8). As a very poor prognostic subtype of CRPC, the five-year survival rate for NEPC patients is only 10% (9). Given the worse prognosis and limited treatment options for CRPC and NEPC, the present study focused on both.

The vascular endothelium controls the entry of nutrients into tissues, maintains blood flow, and regulates the trafficking of white blood cells. Evidence have revealed that abnormalities in the tumor endothelium contribute to tumor growth and metastasis (10). Given the role of blood vessels in maintaining tumors, they have become an increasingly attractive target for the development of anticancer therapies. To improve understanding and manipulation of the relevant pathological mechanisms, researchers must elucidate and exploit the molecular mechanisms of angiogenesis (11,12).

For the aforementioned, the effects of CDK12/insulin like growth factor binding protein 3 (IGFBP3) on cellular biological behavior and angiogenesis in PCa were explored. CDK12 is a serine/threonine protein kinase that regulates transcriptional and post-transcriptional processes, thereby regulating various cellular functions (13). This molecule is critical for the development of cancer (14). After a previous study by the authors identified the pro-oncogenic role of CDK12 in PCa and its negative regulation of another important factor, IGFBP3, the

authors delved into the effect of IGFBP3 on PCa. There are no studies on whether CDK12 plays a role in PCa by inhibiting IGFBP3, thus it was first revealed that CDK12 promotes PCa by inhibiting IGFBP3. IGFBP3 is a proapoptotic, anti-metastatic and antiangiogenic protein that has previously been demonstrated to induce apoptosis using insulin-like growth factor receptor (IGF)-dependent and non-dependent mechanisms (15,16). There have been numerous cancer studies on IGFBP3 as a proapoptotic molecule *in vitro* (17). Growing evidence has revealed that IGFBP regulates angiogenesis (18). After showing that IGFBP3 has a strong inhibitory effect on angiogenesis in PCa (15), the authors subsequently linked CDK12 to angiogenesis and designed experiments to verify the proangiogenic effect of CDK12, which has not been reported by others thus far.

Materials and methods

Cell culture. PCa cells (C4-2 and PC3) and human umbilical vein endothelial cells (HUVECs) were provided by the Institute of Urology, The First Affiliated Hospital of Anhui Medical University (Hefei, China). The minimum number of passages of cells obtained for the first time was 1-2 generations. C4-2 cells were originally isolated from CRPC; PC3 cells were originally isolated from NEPC. PCa cells and HUVECs were cultured in RPMI-1640 medium (cat. no. SH30809.01; HyClone; Cytiva) with 10% fetal bovine serum (cat. no. 086-150; Wisent Biotechnology) and 1% penicillin/streptomycin (cat. no. C0222; Beyotime Institute of Biotechnology). The environment of the cell culture was 37˚C, 5% CO_2, 95% relative humidity. Cells were digested with 0.25% trypsin digestion solution (cat. no. C0201; Beyotime Institute of Biotechnology).

RNA sequencing (RNA-Seq) analysis. The mRNA of C4-2 cells with and without CDK12 knockdown was extracted following the RNeasy Pure mRNA Bead Kit (cat. no. 180244; Qiagen China Co., Ltd.) and the mRNA levels were detected using Duke University's Illumina sequencing platform. The type of sequencing performed was 150 bp for length and 'paired end' for sequencing direction. The loading concentration of the final library was measured using NanoDrop detection at 10 nM. R studio 3.0.1 was used to analyze the data (https://cran-archive.r-project.org/bin/windows/base/old/3.0.1/). The C4-2 cell aliases used in RNA-Seq are LNCaP-C4-2; LNCaP subline C4-2; C4-2; C42; Sp 2817 (cat. no. CRL-3314; American Type Culture Collection). Knockdown of CDK12 in C4-2 cells was performed using CRISPR technology, the oligonucleotides were as follows: forward, 5'-CACCGCGGCGACGTCAGCGACAAAG-3'; and reverse, 5'-AAACCTTTGTCGCTGACGTCGCCGC-3'. Control cells were transfected with the empty vector plasmid Lenti-CRISPR-V2. The oligo sequences were designed using Benchling (https://www.benchling.com). The RNA sequencing data was uploaded to the Gene Expression Omnibus (GEO, https://www.ncbi.nlm.nih.gov/geo/) with the GEO number GSE246983.

CRISPR/CAS9 dual vector lentiviral infection of cells. The products were provided by Shanghai Genechem Co., Ltd. and included Lenti-single guide (sg)RNA-EGFP virus, expressing the target gene sgRNA sequence and control sgRN sequence and Lenti-CAS9-puro virus, expressing the CAS9 protein with puromycin resistance. The CRISPR/CAS9 dual-vector lentivirus enables the knockout of the target gene by introducing the CAS9 protein and the sgRNA sequence expression frame into the cell via two lentiviruses, the CAS9 protein vector with puromycin labeling and sgRNA with a green fluorescent label. C4-2 and PC3 cells were digested and the cell suspension was then seeded in 6-well plates and cultured until the cell confluence reached ~30%. According to the cellular MOI value of 50, an appropriate amount of virus was added. The cell status was observed after 12 h; if there was no obvious cytotoxicity, the medium was replaced after another 24 h; if there was any significant cytotoxicity, the medium was replaced immediately. Three days after infection, an appropriate concentration of puromycin was added to screen for 3 days, after which a low concentration of puromycin was used for continued culture and continued infection with sgRNA lentivirus. The three sgRNA sequences and the control insertion sequences were as follows: PCA09470, 5'-GGGGGAGACAGATCTCCACC-3'; PCA09471, 5'-AGATACAGGGAAAGTAAAGT-3'; PCA09472, 5'-TATGAGATCGTGAGGGACTA-3'; and CON246, 5'-CGCTTCCGCGGCCCGTTCAA-3'. The oligo sequences were designed using the CRISPOR tool version 5.01 (http://crispor.tefor.net/). Cells infected successfully with sgRNA were sorted by green fluorescence. Lenti-CAS9-puro viruses were infected at 37˚C for a duration of at least 3 days and then screened for 3 days with the addition of Puromycin. After that, Lenti-sgRNA-EGFP viruses were infected at 37˚C for a duration of at least 3 days. The duration of cellular infection by both lentiviruses was at least 3 days each. After the Lenti-sgRNA-EGFP viruses were also infected, fluorescence photography revealed the presence of ~80% cells infected. Subsequent experiments were then started. The antibiotic concentration used for selection was 2.00 μg/ml, after which this low concentration was maintained until the Lenti-sgRNA-EGFP viruses had also completed infection. The antibiotic concentration was not maintained after the completion of this experiment.

Transfection of siRNA. RNA primers (20 μM) provided by Shanghai GenePharma Co., Ltd., included: IGFBP3-Homo-915 forward, 5'-GCUGGUGUGUGGAUAAGUATT-3'; and reverse, 5'-UACUUAUCCACACACCAGCTT-3'; and negative control FAM forward, 5'-UUCUCCGAACGUGUCACGUTT-3' and reverse, 5'-ACGUGACACGUUCGGAGAATT-3'. Transfection with siRNA was started when the cell density reached 40 to 70%. Subsequently, 200 μl of Opti-MEM™ I Reduced Serum Medium (cat. no. 31985070; Gibco; Thermo Fisher Scientific, Inc.) was added to each of two DNase/RNase-Free Eppendorf (EP) tubes. One tube had 4 μl of Lipofectamine™ 2000 (cat. no. 11668030; Thermo Fisher Scientific, Inc.) and the other had 8 μl of RNA primers. After incubation for 5 min at room temperature, the contents of the two tubes were mixed and then left to stand for 20 min at room temperature. After the cells were washed with PBS, 1600 μl of serum-free medium was added to each well and the mixture was then added. Cells were cultured in a CO_2 incubator at 37˚C for 6 h and subsequently changed to serum-added medium while the

transfection time was recorded. The time interval between transfection and subsequent experiments was ~24 h.

Co-immunoprecipitation (Co-IP). The Pierce™ Classic Magnetic IP/Co-IP Kit (cat. no. 88804; Thermo Fisher Scientific, Inc.) was used to detect the presence of interactions between CDK12 and IGFBP3. When the density of PC3 cells in the 6-well plate reached 80%, the medium was aspirated and 1 ml of lysis solution was added to one well after two washes with prechilled PBS for 5 min on ice. The cells were scraped off with a cell scraper and the collected cell suspension was added to an EP tube and placed on ice. The samples were centrifuged at 15,000 x g for 10 min at 4˚C. After centrifugation, the supernatant was transferred to a new centrifuge tube, which contained the cell lysate. To reduce the amount of non-specific proteins in the lysate mixture and to reduce the amount of proteins that may cross-react with the protein A/G beads, 1 μl of Goat Anti-Rabbit IgG Antibody (H+L), HRP-conjugated (1:1,000; cat. no. bs-0295G; BIOSS) and 20 μl of Protein A/G beads were added to the cell lysates. The samples were incubated for 30-60 min at 4˚C with rotation and then centrifuged for 1 min at 15,000 x g at 4˚C. The supernatant was transferred to a new EP tube and was set aside. Subsequently, 500 μl of lysate was added to the new EP tube. Anti-IGFBP3 antibody (1:70; cat. no. ab193910; Abcam) was added, mixed gently and then incubated overnight at 4˚C. After the incubation, 20 μl Protein A/G magnetic beads were added, mixed gently and then incubated overnight at 4˚C. Subsequently, the supernatant was discarded after centrifugation at 11,000 x g for 3 min (50 μl of supernatant was retained as 'input') and the immunoprecipitate was retained. The precipitate was washed with 200 μl of lysate, centrifuged at 11,000 x g for 1 min and retained. The sample was then washed once with 100 μl of 1X conditioning buffer (100X for dilution). The precipitate was resuspended in 20 to 40 μl of 2X SDS sample buffer and vortexed. The samples were placed in a metal bath at 100˚C for 5 min and they were finally placed in a centrifuge at 15,000 x g for 1 min. For western blotting, less than 10 μl of sample per well was sufficient.

Western blotting. Proteins were extracted from the cells with RIPA buffer (cat. no. P0013D; Beyotime Institute of Biotechnology) and then separated on 7.5% SDS-polyacrylamide gels (cat. no. P2011; New Cell & Molecular Biotech Co., Ltd.). The samples were then transferred onto PVDF membranes (cat. no. 10600029; Cytiva) or NC membranes (cat. no. 10600002; Cytiva). Non-specific binding was blocked with 5% non-fat milk powder for 2 h at room temperature. Primary antibodies were incubated for 12 h at 4˚C: Anti-β-actin (1:10,000; cat. no. T0022; Affinity Biosciences, Ltd.), anti-CDK12 (1:1,000; cat. no. 11973s; Cell Signaling Technology, Inc.), anti-IGFBP3 (1:1,000; cat. no. ab193910; Abcam), anti-Akt (1:1,000; cat. no. 9272; Cell Signaling Technology, Inc.), anti-p-Akt (1:1,000; cat. no. T40067; Abmart Pharmaceutical Technology Co., Ltd.) and anti-VEGFA (1:1,000; cat. no. 19003-1-AP; ProteinTech Group, Inc.). After incubation with the corresponding secondary antibody (HRP-conjugated Affinipure Goat Anti-Mouse IgG; 1:10,000; cat. no. SA00001-1; ProteinTech Group, Inc. and HRP-conjugated Affinipure goat Anti-Rabbit IgG; 1:10,000; cat. no. SA00001-2; ProteinTech Group, Inc.) for 1 h at room temperature, the protein bands were visualized by an EZ-ECL Kit (cat. no. 20-500-120; Biological Industries) using a gel imaging system (cat. no. AL600RGB; GE Healthcare). Protein band intensities were normalized to that of β-actin. ImageJ software (v.1.8; National Institutes of Health) was used for densitometric analysis.

Reverse transcription-quantitative polymerase chain reaction (RT-qPCR). Total RNA was extracted from the cells of the sgNT group and sgCDK12 group using TRIzol® (Invitrogen; Thermo Fisher Scientific, Inc.). The extracted mRNAs were then subjected to reverse transcription to cDNA (37˚C for 15 min, 85˚C for 5 sec, 4˚C to cool down) by using Evo M-MLV RT Premix for qPCR from Accurate Biotechnology Co., Ltd. (cat. no. AG11706). The SYBR® Green Premix Pro Taq HS qPCR kit (cat. no. AG11701; Accurate Biotechnology Co., Ltd.) assisted in quantifying obtained cDNAs, and 7500 Software v.2.3 on Applied Biosystems™ 7500 Real-Time PCR System (Applied Biosystems; Thermo Fisher Scientific, Inc.) was adopted to detect quantified cDNAs. The qPCR conditions were as follows: Initial denaturation at 95˚C for 30 sec; followed by 40 cycles of denaturation at 95˚C for 5 sec; annealing at 60˚C for 30 sec and finally a system default dissociation stage. The $2^{-\Delta\Delta Cq}$ method was used to quantify the fold change in gene expression (19). Primers were provided by Sangon Biotech Co., Ltd. The sequences of the primers were as follows: CDK12 forward, 5'-CTAACAGCAGAGAGCGTCACC-3' and reverse, 5'-AAAGGTTTGATAACTGTGCCCA-3' (20); IGFBP3 forward, 5'-TGTGGCCATGACTGAGGAAA-3' and reverse, 5'-TGCCGACCTTCTTGGGTTT-3' (21); and GAPDH forward, 5'-CATGAGAAGTATGACAACAGCCT-3' and reverse 5'-AGTCCTTCCACGATACCAAAGT-3' (22).

Cell proliferation assay. Cell proliferation was detected using Cell Counting Kit-8 (CCK-8; cat. no. C0005; TopScience) and EdU assays (cat. no. C0071S; Beyotime Institute of Biotechnology). Cell suspensions of the sgNT group, sgCDK12 group and siIGFBP3/sgCDK12 group were spread in five 96-well plates with $5x10^3$ cells per well for the C4-2 cell line and $2x10^3$ cells per well for the PC3 cell line. CCK-8 reagent was added at 10:1 at 0, 24, 48, 72 and 96 h and incubated in the dark at 37˚C for 2 h. Absorbance was measured at 450 nm wavelength using a microplate reader (PerkinElmer, Inc.). Cell suspensions of the sgNT group, sgCDK12 group and siIGFBP3/sgCDK12 group were spread overnight in 24-well plates at $8x10^4$ cells per well. Cells were labeled with EdU, and 100 μl of click reaction solution was added to each well and incubated at room temperature for 30 min in the dark. Finally, the cells were stained with Hoechst 33342 for nuclear staining. EdU labeling and Hoechst staining were examined using fluorescence microscopy (Carl Zeiss AG). The fluorescence intensity of the EdU-labeling proliferation assay was quantified by ImageJ software (v.1.8; National Institutes of Health).

Colony formation assay. Cells from the sgNT group, sgCDK12 group and siIGFBP3/sgCDK12 group were digested and spread into 6-well plates at $5x10^3$ cells per well for the C4-2 cell line and $1x10^3$ cells per well for the PC3 cell line. The medium was

changed every 2-3 days. After 14 days at 37˚C, the medium was discarded and the cell colonies were fixed with 4% paraformaldehyde at room temperature for 30 min and stained with crystal violet staining solution (cat. no. C0121; Beyotime Institute of Biotechnology) at room temperature for 15 min. Colonies consisting of >50 cells were counted with ImageJ software (v.1.8; National Institutes of Health).

Cell migration assay. Cell migration was detected using Transwell migration assays and wound healing assays. Cell suspensions of the sgNT group, sgCDK12 group and siIGFBP3/sgCDK12 group were spread equally into Petri dishes. When the cell density reached the same level, the medium was discarded in the dish and then three straight lines of equal thickness on each dish were scratched with a 10-μl pipette tip. After PBS washes, serum-free medium was added. Images were captured at x40 magnification using a light microscope (Olympus Co.) at 0, 24, 48, 72 and 96 h after scratching to compare the wound healing ability of different cell lines. The wound closures were calculated by ImageJ software. Transwell migration assays were performed using a 24-well Transwell system (cat. no. 3495; Corning, Inc.). Cells from the sgNT group, sgCDK12 group and siIGFBP3/sgCDK12 group were digested and then resuspended in serum-free medium. A total of $1x10^5$ cells were added into each upper chamber. Subsequently, 600 μl of serum-containing medium was added to the lower chambers. The cells were incubated in a CO_2 incubator at 37˚C for 24 h. The cells crossing the membrane were fixed with 4% paraformaldehyde at room temperature for 30 min and then stained with 100% crystal violet staining solution at room temperature for 15 min. Cells crossing the membrane were counted by ImageJ software after taking pictures under a light microscope (magnification, x40 and x100; Olympus Corporation).

Tube formation assay. The cell supernatant from the sgNT group, sgCDK12 group and siIGFBP3/sgCDK12 group was taken as the conditioned medium in advance. The materials that would come in contact with the Matrigel matrix (cat. no. 356234; Corning, Inc.) were precooled. When HUVECs grew to 70-90% confluence, the medium was changed to serum-free medium. A total of 50 μl of Matrigel matrix per well was added to a 96-well plate and then placed into the incubator for 30 min to solidify the Matrigel matrix. HUVECs were resuspended in ~1 ml of conditioned medium to adjust their density to $3x10^5$ cells/ml. A total of 100 μl of cell suspension was placed in each well and the time was recorded as 0 h after plating. Images were captured using a light microscope (Olympus Corporation) at x40 magnification at 2, 4 and 6 h. The total tubule length was calculated using ImageJ software.

Immunohistochemistry (IHC). Specimens were fixed in 10% neutral formalin at room temperature for 48 h, paraffin-embedded and ultramicro-sectioned to 3-μm thick. Slices were dewaxed with xylene, rehydrated with graded alcohol and incubated with 3% Peroxidase Closure Solution (cat. no. ZLI-9311; Beijing Zhongshan Golden Bridge Biotechnology Co., Ltd.) at room temperature for 30 min to block endogenous peroxidase activity. Slices were repaired with citrate repair solution (cat. no. ZLI-9064; Beijing Zhongshan Golden Bridge Biotechnology Co., Ltd.) at high pressure to repair antigen and incubated overnight in an IHC wet box at 4˚C with anti-CDK12 (1:50; cat. no. ab246887; Abcam), anti-IGFBP3 (1:80; cat. no. ab193910; Abcam), anti-VEGFA (1:200; cat. no. 19003-1-AP; ProteinTech Group, Inc.) and anti-CD31 (1:2,000; cat. no. ab182981; Abcam) antibodies. The next day, slices were washed with PBS and incubated with HRP-labeled anti-rabbit IgG (100%; cat. no. DS-0004; Beijing Zhongshan Golden Bridge Biotechnology Co., Ltd.) at room temperature for 1 h. Immunoreactivity was detected with the DAB kit (cat. no. ZLI-9018; Beijing Zhongshan Golden Bridge Biotechnology Co., Ltd.), and the sections were then observed under a light microscope (magnification, x100 and x400; Olympus Corporation). Scores for CDK12, IGFBP3, and VEGFA staining intensity were defined as follows: negative, 0 points; weakly positive, 1 point; moderate, 2 points; and strongly positive, 3 points. The frequency of positive cells was defined as follows: less than 5%, 0 points; 5-25%, 1 point; 26-50%, 2 points; 51-75%, 3 points and more than 75%, 4 points. CD31 IHC staining was used to determine the microvessel density (MVD) by first finding the densest area of microvessels with a x10 objective and subsequently to assess the number of microvessels in the x20 objective field.

Hematoxylin-eosin (H&E) staining. Specimens were fixed in 10% neutral formalin at room temperature for 48 h, paraffin-embedded and ultramicro-sectioned to 3-μm thick. Slices were dewaxed with xylene and rehydrated with graded alcohol. Subsequently, slices were stained with H&E using standard procedures. Hematoxylin staining was used for 5 min at room temperature and eosin staining was used for 2 min at room temperature. The sections were then observed under a light microscope (magnification, x100 and x400; Olympus Corporation).

LinkedOmics database. The LinkedOmics database (http://www.linkedomics.org.) is a publicly available portal that includes multiomics from all 32 cancer types in The Cancer Genome Atlas (TCGA) and 10 from Clinical Proteomics Tumor Analysis Consortium (CPTAC) cancer cohort data. After identification of the 'prostate adenocarcinoma' type, the following analysis was performed on September 27, 2022, according to the 'Manual and Tutorial' on the website: Pearson correlation coefficient between CDK12 and IGFBP3, Pearson correlation coefficient between CDK12 and VEGFA, Pearson correlation coefficient between IGFBP3 and VEGFA, and the relationship between CDK12, IGFBP3 and overall survival (OS) in patients with PCa.

In vivo tumor assays. The cells of the PC3/sgNT group and PC3/sgCDK12 group were suspended in serum-free medium. Six-week-old male BALB/c nude mice (weight, 25-30 g; 3 mice/group; Jiangsu Huachuang Xinnuo Pharmaceutical Technology Co, Ltd.) were injected subcutaneously with 300 μl and $1x10^7$ cells each. The cells were placed on ice at all times during the injection. The protocol for the animal experiments was approved by the Experimental Animal Ethics Committee of Anhui Medical University (approval no. LLSC20190458). Mice were housed under specific pathogen-free conditions

at 25˚C with a 12 h light/dark cycle and free access to food and water. Tumor size and mouse weight were measured every 3 days after feeding until the tumor was visible to the naked eye and started to be recorded as Day 0. Tumor growth was calculated using the following formula: Volume =0.52x length x width^2. When the tumors were nearly 15 mm in diameter, the mice were sacrificed using the spinal dislocation method. The tumors were taken from the mice, weighed and preserved.

Statistical analysis. All experiments had three independent replicates, and the data were presented as the mean ± SD. ImageJ software (v.1.8; National Institutes of Health) was used for densitometric analysis. Statistical analyses were performed using GraphPad Prism 8.0.2 software (GraphPad Software; Dotmatics). Comparisons between two groups were performed using a two-tailed unpaired Student's t-test, and multiple groups were analyzed by one-way ANOVA followed by Tukey's post hoc test for further pairwise comparisons. Pearson's correlation coefficient was used to study the relationship between variables. In all cases, $P<0.05$ was considered to indicate a statistically significant difference.

Results

Role of CDK12 in the regulation of IGFBP3. After knocking down CDK12 in C4-2 PCa cells, mRNA of the C4-2 cells from the knockdown group and control group was sequenced and the results are illustrated in a heatmap. The heatmap revealed that IGFBP3 was significantly upregulated after CDK12 was knocked down (Fig. 1A). Subsequently, the Pearson correlation coefficient between CDK12 and IGFBP3 was analyzed in the LinkedOmics database (http://www.linkedomics.org): There was a negative correlation between CDK12 and IGFBP3 (Fig. 1B). Therefore, it was hypothesized that CDK12 can inhibit the expression of IGFBP3 in anterior adenocarcinoma cells. To further verify this conjecture, the interaction between IGFBP3 protein and CDK12 protein by co-IP was assessed (Fig. 1C). Next, the CRISPR/CAS9 technique was used to stably knock out CDK12 in PCa cells to further observe the relationship between CDK12 and IGFBP3. RNA and protein were extracted from the sgNT group and sgCDK12 group for RT-qPCR and western blotting, respectively. The assay results demonstrated that CDK12 was knocked down in the sgCDK12 group of cells and it was revealed that IGFBP3 in the sgCDK12 group was higher at both the RNA and protein levels than that in the sgNT group (Fig. 1D and E). In summary, these findings indicated that CDK12 plays a negative regulatory role on IGFBP3 in PCa cells.

CDK12 promotes the proliferation, colony formation and migration of PCa cells by inhibiting IGFBP3. To clarify the role of CDK12/IGFBP3 in PCa cells, IGFBP3 was knocked down on the basis of knocking out CDK12, resulting in three groups of cells: i) sgNT group, ii) sgCDK12 group and iii) siIGFBP3/sgCDK12 group. These three groups of cells were used for CCK-8, EdU and colony formation assays. CCK-8 assays demonstrated that the proliferation ability of PCa cells decreased after the knockout of CDK12; on the basis of knocking out CDK12, the cell proliferation of the IGFBP3 knockdown group was restored (Fig. 2A and B). EdU assays revealed that the EdU positive ration decreased after the knockout of CDK12; on the basis of knocking out CDK12, the EdU positive ration of the IGFBP3 knockdown group was restored (Fig. 2C and D). Colony formation assays showed that the number of cell colonies was reduced after the knockout of CDK12; on the basis of knocking out CDK12, the number of the IGFBP3 knockdown group was restored (Fig. 2E and F). Transwell migration and wound healing assays were subsequently performed. Transwell migration assays revealed that the intensity of cells through a porous membrane decreased after CDK12 was knocked out; on the basis of knocking out CDK12, the intensity of IGFBP3 knockdown group was restored (Fig. 3A and B). Wound healing assays demonstrated that the migration of PCa cells decreased after CDK12 was knocked out; on the basis of knocking out CDK12, the cell migration of IGFBP3 knockdown cells was restored (Fig. 3C and D). In addition, the relationship between CDK12, IGFBP3 and OS in PCa patients was analyzed separately in the LinkedOmics database. The results indicated that patients with CDK12 above the median had shorter OS (P=0.9739) (Fig. S1A) while patients with IGFBP3 above the median had longer OS (P=0.679) (Fig. S1B). Therefore, it was inferred that CDK12 promotes the proliferation, cloning and migration of PCa cells and that IGFBP3 inhibits the proliferation, cloning and migration of PCa cells. Furthermore, the aforementioned cell behavioral effects of CDK12 on PCa are accomplished through the inhibition of IGFBP3 expression.

CDK12 promotes angiogenesis and expression of related signal molecules in PCa by inhibiting IGFBP3. After initially elucidating the effects of CDK12/IGFBP3 on the cellular biological behavior of PCa, the authors investigated the effects of CDK12/IGFBP3 on PCa angiogenesis. The Pearson correlation coefficients were analyzed between CDK12, IGFBP3 and VEGFA in patients with PCa patients separately in the LinkedOmics database: CDK12 was positively correlated with VEGFA, while IGFBP3 was negatively correlated with VEGFA (Fig. 4A). Then, the regulatory effects of CDK12/IGFBP3 on Akt (protein kinase B) activity and VEGFA expression were analyzed using western blot analysis. CDK12 was found to activate Akt and upregulate VEGFA in the sgNT group vs. the sgCKD12 group; IGFBP3 was found to inhibit Akt activity and downregulate VEGFA in the sgCDK12 group vs. the siIGFBP3/sgCKD12 group (Fig. 4B). The phosphorylation level of Akt and the expression level of VEGFA in the siIGFBP3/sgCKD12 group were both increased compared with those of the sgCDK12 group (Fig. 4B), thus, the authors inferred that CDK12 activates Akt and promotes VEGFA expression by inhibiting IGFBP3. The results of the tube formation assay demonstrated that the total tubule length decreased after CDK12 knockdown, while the total tubule length increased again after knockdown of CDK12 and IGFBP3 to a level that was not significantly different from that of the sgNT group (Fig. 4C and D). This finding further validated that CDK12 can promote PCa angiogenesis by inhibiting IGFBP3.

Results of tumorigenic experiments in nude mice. After transplanting equal amounts of sgNT and sgCDK2 group cells into nude mice subcutaneously, the tumor size and nude mouse body weight were recorded every three days after tumor

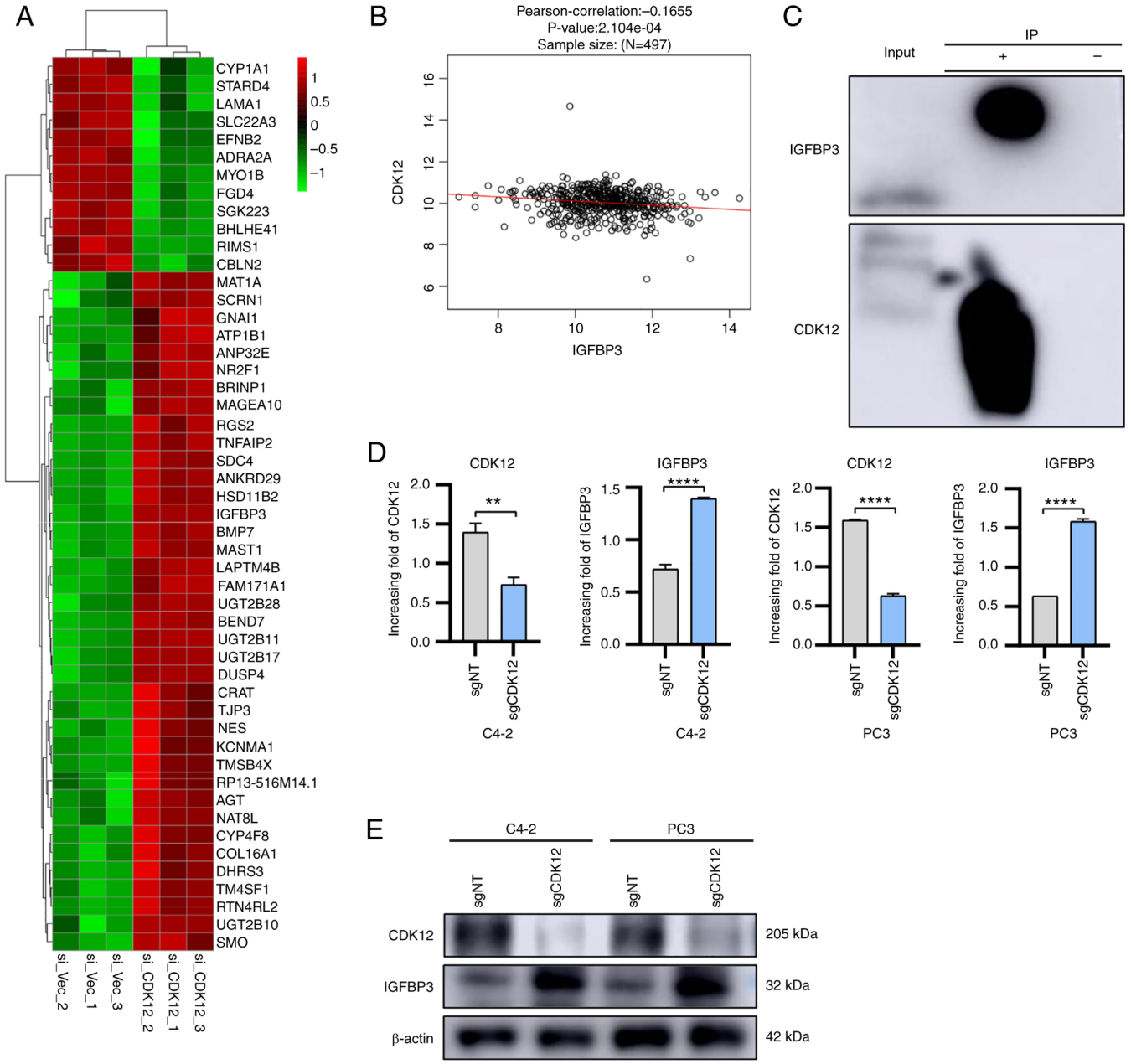

Figure 1. Role of CDK12 in the regulation of IGFBP3. (A) CDK12 was knocked down in C4-2 cells. The mRNA levels of C4-2 cells with and without CDK12 knockdown were detected using Duke University's Illumina sequencing platform. (B) The Pearson correlation coefficient between CDK12 and IGFBP3 was analyzed in the LinkedOmics database. (C) PC3 cellular proteins were extracted and used to analyze the interaction between CDK12 and IGFBP3 by co-immunoprecipitation. The target protein (IGFBP3) and its binding partner (CDK12) were co-precipitated using anti-IGFBP3 antibody. Total RNA and proteins of cells (C4-2 and PC3) from sgNT group and sgCDK12 group were extracted. (D) RNA expression of CDK12 and IGFBP3 was detected by reverse transcription-quantitative PCR. (E) Expression of CDK12 and IGFBP3 proteins was detected by western blotting. β-actin was used as an internal control. Two-tailed unpaired Student's t-test was used. **P<0.01 and ****P<0.0001. IGFBP3, insulin like growth factor binding protein 3; si, small interfering; sg, single guide; si_CDK12, C4-2 cells with CDK12 knockdown; si_Vec, C4-2 cells without CDK12 knockdown; sgNT group, group without knockdown of CDK12 and IGFBP3 in cells; sgCDK12 group, group with knockdown of CDK12 using CRISPR technology; siIGFBP3/sgCDK12 group, group with knockdown of CDK12 using CRISPR technology and knockdown of IGFBP3 by transfection with siRNA; IP, immunoprecipitation.

formation. The transplanted tumors in the sgNT group gradually increased in size, while those in the sgCDK12 group grew slowly with minimal volume changes (Fig. 5B). Nude mice were sacrificed to remove the tumors when the largest tumor was close to 150 mm in diameter. Visual observation revealed that the tumor volume of nude mice in the sgNT group was larger than that in the sgCDK12 group; weighing of the transplanted tumors revealed that the weight of the sgNT group was larger than that of the sgCDK12 group (Fig. 5A and B). The transplanted tumors were embedded into wax blocks and then sliced for H&E and IHC, which showed lower CDK12 expression in the sgCDK12 group (Fig. 5C and D). The MVD of the tissues was counted after incubation with anti-CD31 antibodies and the MVD was 17, 29 and 19/field of view at x200 magnification for the sgNT group and 7, 8 and 9/field of view at x200 magnification for the sgCDK12 MVD (Fig. 5F). After incubation with anti-IGFBP3 antibodies and anti-VEGFA antibodies, the results revealed that IGFBP3 expression in

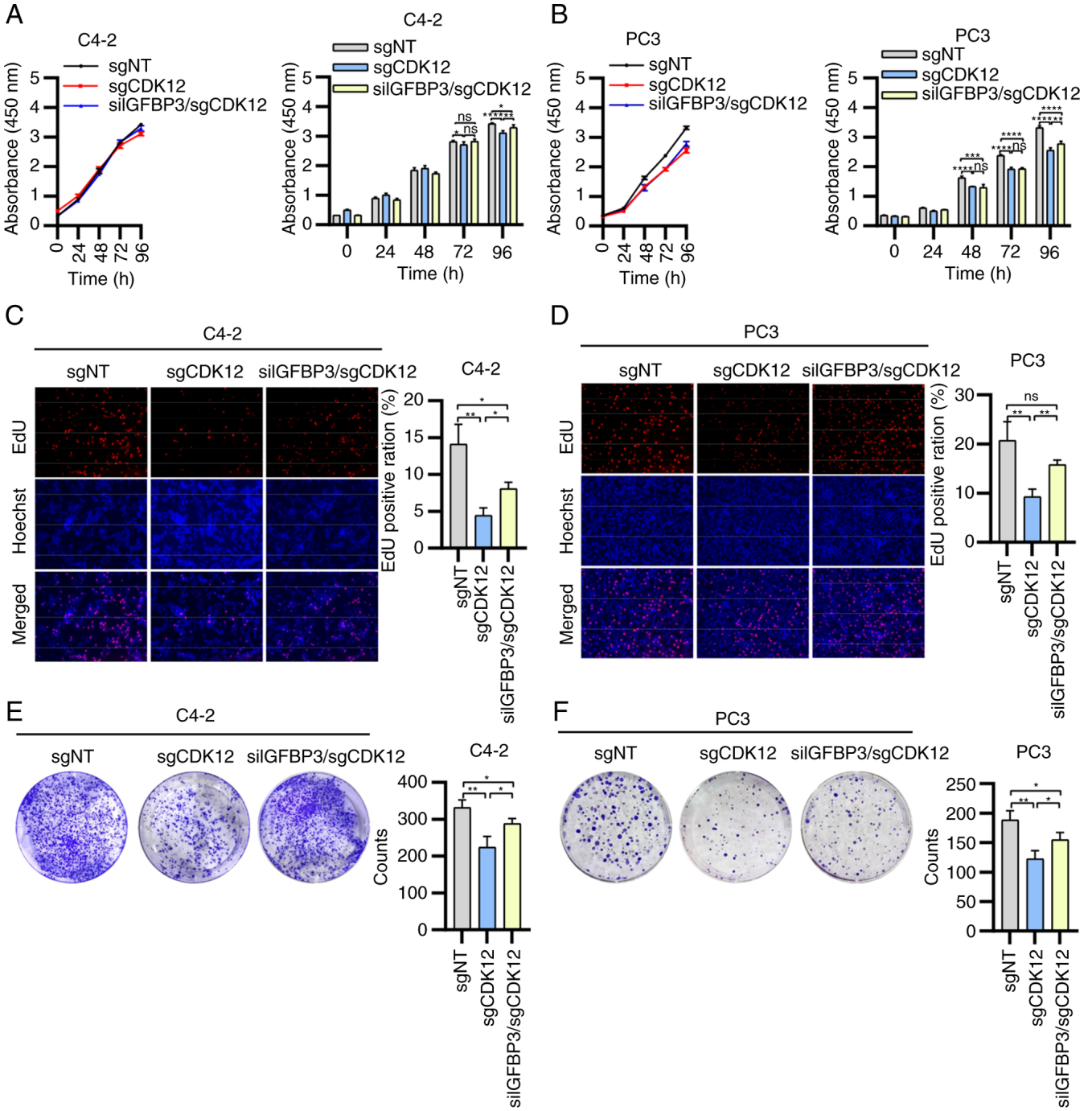

Figure 2. Effect of CDK12/IGFBP3 on cell proliferation in advanced prostate cancer. Cells (C4-2 and PC3) from the sgNT group, sgCDK12 group and siIGFBP3/sgCDK12 group were cultured simultaneously in culture dishes of different specifications. (A and B) Cell proliferation was analyzed by Cell Counting Kit-8 assays, (C and D) EdU and (E and F) colony formation assays. (C and D) Fluorescence microscopy of EdU and Hoechst stains. Magnification, x40. Two-tailed unpaired Student's t-test was employed. *P<0.05, **P<0.01, ***P<0.001 and ****P<0.0001. IGFBP3, insulin like growth factor binding protein 3; si, small interfering; sg, single guide; sgNT group, group without knockdown of CDK12 and IGFBP3 in cells; sgCDK12 group, group with knockdown of CDK12 using CRISPR technology; siIGFBP3/sgCDK12 group, group with knockdown of CDK12 using technology and knockdown of IGFBP3 by transfection with siRNA; ns, not significant.

the sgNT group was lower than that in the sgCDK12 group (Fig. 5E) and VEGFA expression was higher than that in the sgCDK12 group (Fig. 5G).

Discussion

CDKs are a family of serine/threonine kinases. Based on their regulatory functions, CDKs can be functionally subdivided into CDKs related to cell cycle processes and CDKs related to transcription (23). CDK12 is located on chromosome 17, contains 14 exons and encodes a protein of ~164 kDa consisting of 1,490 amino acids (24). CDK12 consists of different functional structural domains: a centrally located kinase domain, several RS (arginine/serine) patterns near the N-terminus and a proline-rich pattern, which can act as a binding site for other proteins (25). CDK12 is considered to regulate gene

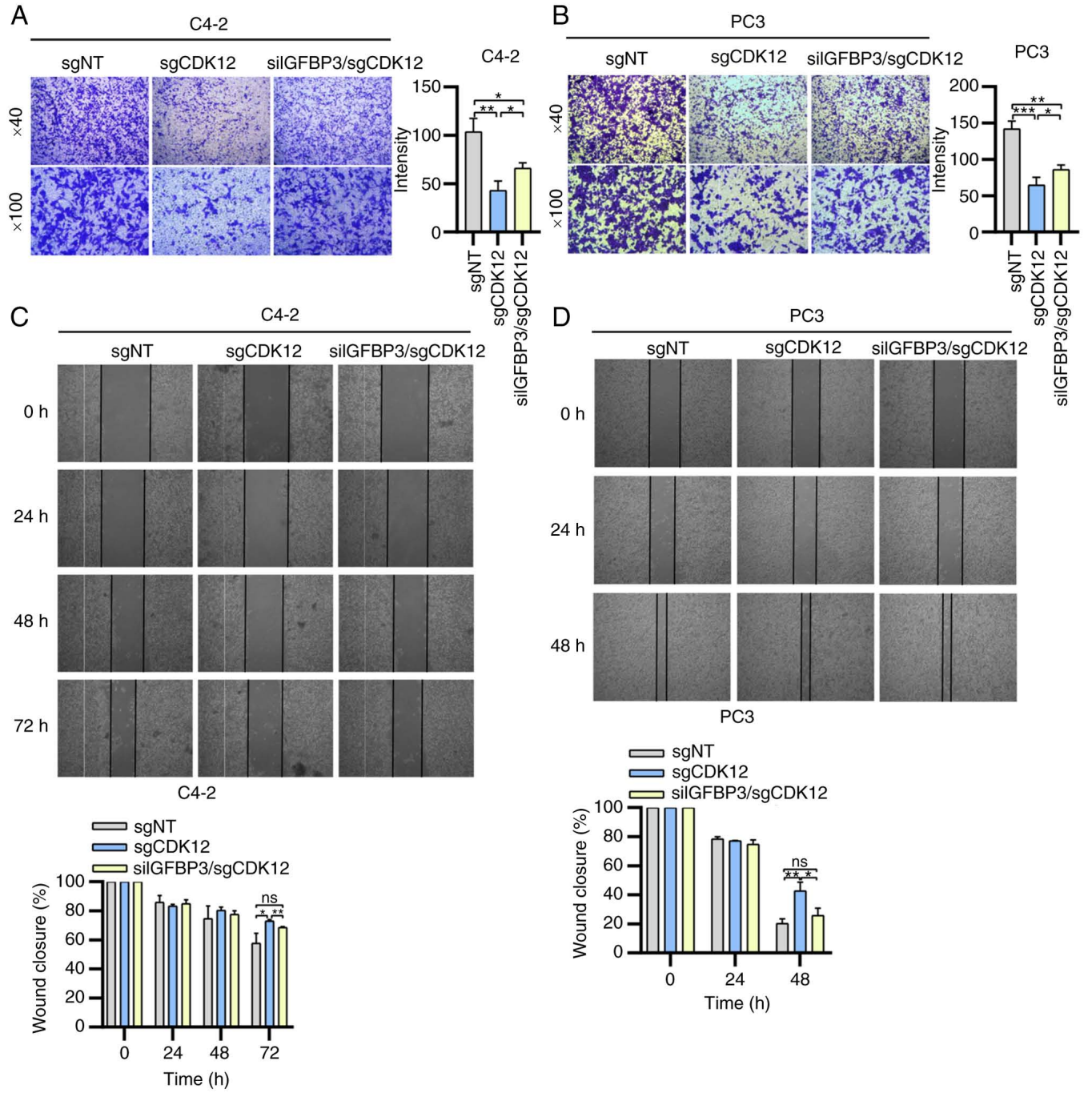

Figure 3. Effect of CDK12/IGFBP3 on cell migration in advanced prostate cancer. The migration of cells (C4-2 and PC3) from the sgNT group, sgCDK12 group and siIGFBP3/sgCDK12 group was examined by (A and B) Transwell migration assays and (C and D) wound healing assays using light microscopy. Magnification, x40 and x100 for Transwell migration assays. Magnification, x40 for wound healing assays. Two-tailed unpaired Student's t-test was employed. *P<0.05; **P<0.01 and ***P<0.001. IGFBP3, insulin like growth factor binding protein 3; si, small interfering; sg, single guide; sgNT group, group without knockdown of CDK12 and IGFBP3 in cells; sgCDK12 group, group with knockdown of CDK12 using CRISPR technology; siIGFBP3/sgCDK12 group, group with knockdown of CDK12 using CRISPR technology and knockdown of IGFBP3 by transfection with siRNA; ns, not significant.

transcription by phosphorylating RNA polymerase II, which can directly regulate transcription by phosphorylating serine residues within the C-terminal structural domain of RNA polymerase II (YSPTSPS), which is essential for transcriptional elongation (25,26). In the present study, significant changes were first observed in IGFBP3 after CDK12 was knocked down, as shown by RNA-seq, and several studies have reported a strong association between IGFBP3 and angiogenesis (21,27-29). Subsequently, the study of CDK12/IGFBP3 in PCa was initiated. The human IGFBP3 gene is located on the short arm of chromosome 7 and has five exons. In the N-terminal region of IGFBP3, there are post-translational modification sites; in addition, there are many phosphorylation sites and three glycosylation sites (30). Despite the high long-term survival rates of localized PCa, metastatic PCa remains largely incurable, even after intensive multimodal therapy (3). Therefore, in the present study, a series of *in vivo* and *in vitro* experiments were conducted to study the biological behavior of mid-to-late stage

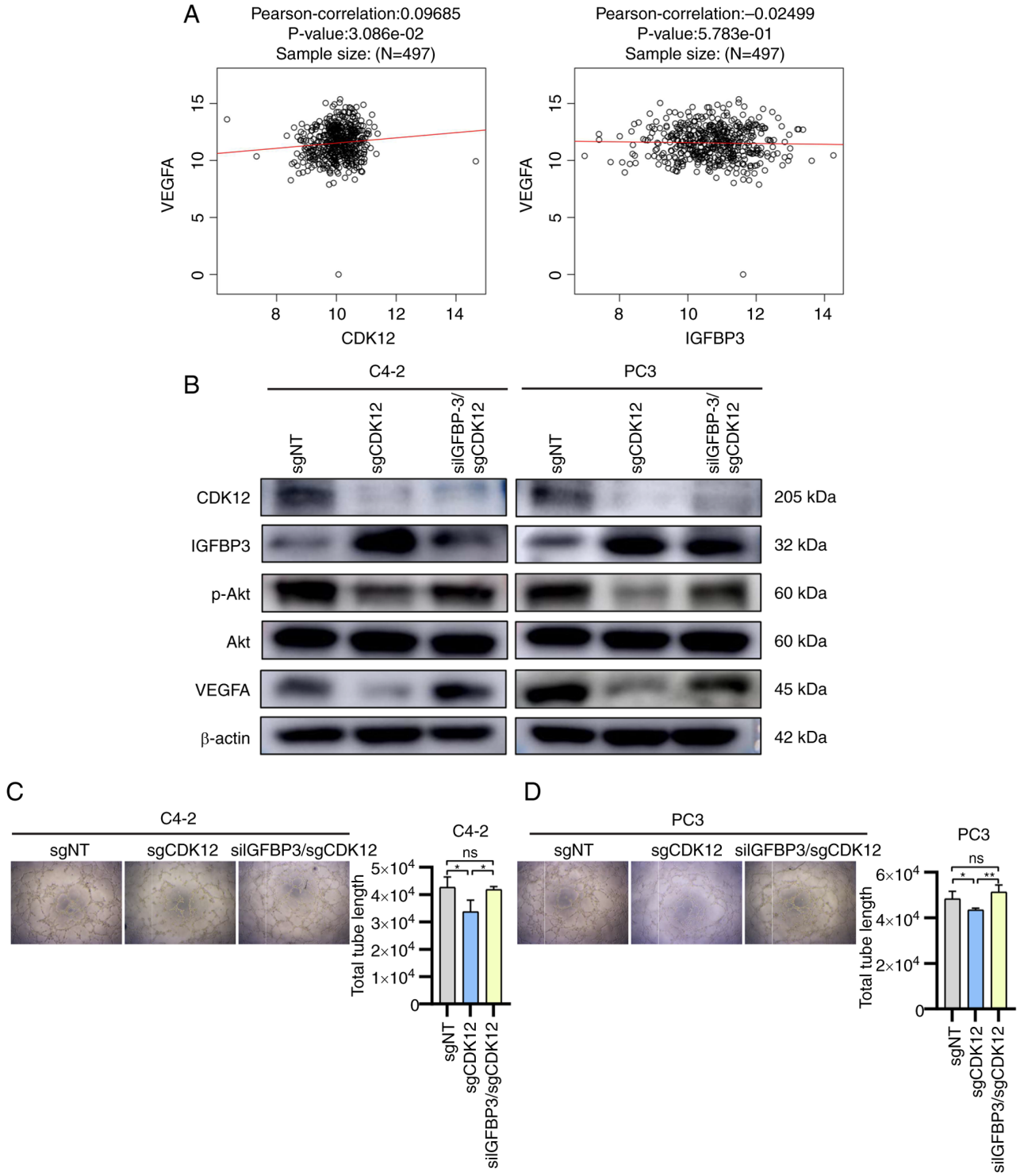

Figure 4. Effect of CDK12/IGFBP3 on angiogenesis and expression of related signal molecules in advanced prostate cancer. (A) Pearson correlation coefficients between CDK12 and VEGFA and between IGFBP3 and VEGFA were analyzed in the LinkedOmics database. (B) Total proteins of cells (C4-2 and PC3) from the sgNT group, sgCDK12 group and siIGFBP3/sgCDK12 group were extracted and protein levels of CDK12, IGFBP3 and angiogenesis-related signals were measured by western blotting. β-actin was used as an internal control. (C and D) Supernatant of sgNT group, sgCDK12 group and siIGFBP3/sgCDK12 group cells (C4-2 and PC3) were collected. Equal amounts of HUVECs were resuspended with the supernatant for culture. Using light microscopy after 6 h. Magnification, x40. Two-tailed unpaired Student's t-test was used. *P<0.05 and **P<0.01. IGFBP3, insulin like growth factor binding protein 3; si, small interfering; sg, single guide; sgNT group, group without knockdown of CDK12 and IGFBP3 in cells; sgCDK12 group: group with knockdown of CDK12 using CRISPR technology; siIGFBP3/sgCDK12 group, group with knockdown of CDK12 using CRISPR technology and knockdown of IGFBP3 by transfection with siRNA; HUVECs, human umbilical vein endothelial cells; ns, not significant.

PCa cells from Chinese men and their proteins and RNAs were extracted to observe the alteration of the target molecules. The C4-2 cells demonstrate CRPC characteristics and PC3 cells demonstrate NEPC characteristics. Lack of the employment of more cell lines constituted a limitation of the present study. Proteins from PC3 cells were extracted for co-IP and the results

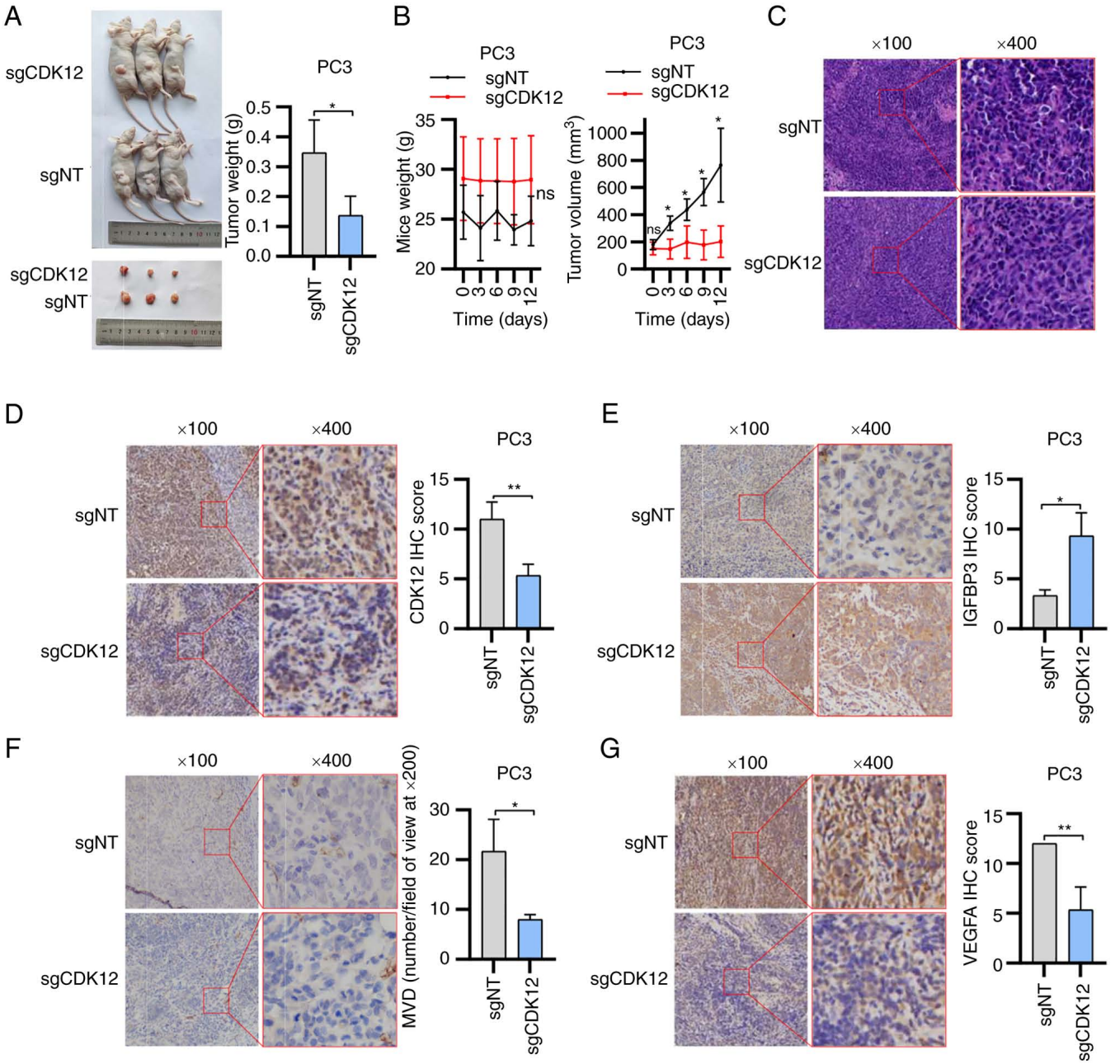

Figure 5. Results of tumorigenic experiments in nude mice. (A) Nude mice and subcutaneous xenograft tumor images. (B) Tumor volume change in mice and weight comparison after removal. (C) Tumor blocks were sectioned and stained for hematoxylin-eosin staining. Immunohistochemistry was used to detect the expression of (D) CDK12, (E) IGFBP3, (F) CD31 and (G) VEGFA in sgNT group tissues and in sgCDK12 group tissues by using light microscopy. Magnification, x100 and x400. Two-tailed unpaired Student's t-test was used. *P<0.05 and **P<0.01. IGFBP3, insulin like growth factor binding protein 3; si, small interfering; sg, single guide; sgNT group, group without knockdown of CDK12 and IGFBP3 in cells; sgCDK12 group, group with knockdown of CDK12 using CRISPR technology; siIGFBP3/sgCDK12 group, group with knockdown of CDK12 using CRISPR technology and knockdown of IGFBP3 by transfection with siRNA; ns, not significant; MVD, microvessel density.

revealed that CDK12 interacts with IGFBP3 in a protein-protein mechanism. However, this finding did not yet indicate a direct regulatory relationship between CDK12 and IGFBP3, this is also a limitation of the present study, while there may be a third interacting protein between them (31). Western blot analysis was also employed and revealed that CDK12 inhibits the protein expression of IGFBP3. RT-qPCR results revealed that CDK12 also inhibits the mRNA synthesis of IGFBP3. The correlation between CDK12 and IGFBP3 mined from the LinkedOmics database is consistent with the aforementioned experimental results.

A number of studies have revealed that patients with CDK12 deletion mutations have shorter OS than patients with wild-type CDK12 (32-34). However, a different study used a CRISPR screen to find that CDK12 is required for PCa cell survival. CDK12 accelerates the progression of PCa to some extent. Some researchers verified the dependence of PCa cells on CDK12 from the Project Score; the mRNA level of CDK12 was found to be significantly higher in PCa than in normal prostate tissue from Tomlins; in addition, researchers found from TCGA data that patients with PCa with lower CDK12 mRNA levels had slightly longer disease-free survival (35).

In a study conducted by Wu *et al* (25), cell proliferation was observed to be decreased following CDK12 knockdown by kinetic imaging confluence measurements conducted at 3-h intervals. Furthermore, Wu *et al* (25) suggested that CDK12 deficiency may result in elevated T cell infiltration. It is possible that inconsistent findings regarding CDK12 are due to various factors, including the absence of patient-derived T cells in culture dishes or in nude mice, which may necessitate further investigation. Regarding IGFBP3, this protein inhibits cell proliferation and stimulates apoptosis (36). IGFBP3 overexpression has been demonstrated to induce G1 phase cell cycle arrest and inhibit PCa metastasis in breast cancer (37). The antitumor activity and mechanism of action of IGFBP3 have also been extensively validated in various preclinical model systems (38-40). A previous *in vitro* study in PCa have also revealed that IGFBP3 independently inhibits PCa cell growth and promotes apoptosis (41). In addition, many of the roles of IGFBP3, including inhibition of the NF-kB pathway, appear to be independent of its ability to isolate IGF. Low IGFBP3 in serum is associated with a risk of more aggressive PCa (16). To confirm the essential role of CDK12 in PCa, CRISPR/CAS9 was used to knock down CDK12 in the two PCa cell lines aforementioned. Preliminary studies by the authors have confirmed that CDK12 negatively regulates IGFBP3. Therefore, the expression of IGFBP3 in cells was knocked down using siRNA in addition to the knockdown of CDK12 so that it could be analyzed whether the effect of CDK12 on PCa cells is related to IGFBP3. Both the CCK-8 assay and EdU assay results indicated that CDK12 promoted PCa cell proliferation by inhibiting IGFBP3. Because the expression of IGFBP3 was upregulated after CDK12 was knocked down, the proliferation of PCa cells was diminished at this time and after knocking down CDK12, the expression of IGFBP3 was simultaneously knocked down and it was found that the cell proliferation was restored. The EdU assay revealed that there was no longer a significant difference in the proliferative capacity of PC3 cells between the sgNT group and the siIGFBP3/sgCDK12 group. In parallel, a colony formation assay was performed as a corroboration of the first two proliferation assays. The results reinforced the conclusion that CDK12 promotes the proliferation of PCa cells by inhibiting IGFBP3. The effect of CDK12/IGFBP3 on the migration of PCa cells was then investigated by Transwell migration and wound healing assays. The knockdown of CDK12 reduced the number of cells crossing the membrane and slowed the rate of wound closure. The cell migration ability was restored after simultaneous knockdown of IGFBP3. The wound healing assay demonstrated that there was no longer a significant difference in the migratory capacity of PC3 cells between the sgNT group and the siIGFBP3/sgCDK12 group. The authors thus concluded that CDK12 promotes PCa cell migration by inhibiting IGFBP3.

Blood vessels form the largest network in the human body, and when dysregulated, the formation of new blood vessels can lead to many malignant, ischemic, inflammatory, infectious and immune diseases (10,42). Angiogenesis is a key feature in tumorigenesis and remains a potential target for antiangiogenic therapy (43). Angiogenesis divides the development of any solid tumor into two stages: The avascular stage and the vascular stage. Because of this, angiogenesis plays a key role in the biology of solid tumors. If this vascular growth can be stopped by interrupting the tumor signals that trigger capillary proliferation, the small tumor population will remain dormant, similar to normal cells, relying on the diffusion principle to absorb nutrients and release catabolites. If this phenomenon can be achieved, it may become an effective therapy in its own right or a powerful adjunct to other treatments (44). However, antiangiogenic therapies have also revealed that resistance to antiangiogenic drugs readily arises and may involve alterations in vascular signaling mechanisms (45). There is still a gap in the reports of CDK12 in relation to angiogenesis, but there are many vascular reports on IGFBP3 and angiogenesis. IGFBP3, a serum component associated with angiogenesis, has been reported to have pro- and antiangiogenic effects (46). IGFBP3 has been suggested to promote cell migration and angiogenesis in endothelial precursor cells (47). IGFBP3 also enhanced the mRNA expression and protein secretion of VEGF in HUVECs (48). IGFBP3 reduced cellular capillary formation in HUVECs and reduced angiogenesis in chick embryonic chorionic villus assays and xenografts of IGFBP3 transfectants significantly reduced tumor growth and angiogenesis (21). The farnesyltransferase inhibitor (FTI) SCH66336 has been demonstrated to have antitumor activity against head and neck squamous cell carcinoma (HNSCC) *in vitro* and *in vivo*. A previous study suggested that IGFBP3 may be a major target for the antitumor activity of FTIs and that IGFBP3 is an effective treatment for HNSCC angiogenesis (18). In addition, IGFBP3 inhibited the adhesion of HNSCC cells and HUVECs to the extracellular matrix, in part by negatively regulating integrin β4 expression in an IGF-dependent and IGF-independent manner. These data explain how IGFBP3 regulates cancer cell metastasis and tumor angiogenesis (49). The LinkedOmics database was investigated and it was observed that IGFBP3 was negatively correlated with VEGFA, which is consistent with the aforementioned findings of others; CDK12 was also found to be positively correlated with VEGFA, which is consistent with the authors' expectations. VEGF is a growth factor with important proangiogenic activity and has mitogenic and antiapoptotic effects on endothelial cells. VEGFA, also known as VEGF, is the most important and potent angiogenesis stimulating factor (50). Akt is closely linked to VEGF, and Akt, also known as protein kinase B (PKB), is a serine/threonine kinase involved in several key cellular pathways, including proliferation, invasion, apoptosis and angiogenesis (51,52). Akt1 is essential for VEGF-induced angiogenesis (53). Akt can also promote tumor angiogenesis by activating nitric oxide in the endothelium (54). Akt and VEGF form an autocrine circuit in cells that regulates angiogenesis, where VEGF activates the Akt signaling pathway, which in turn regulates the expression of VEGF and its receptors. Activation of Akt also induces the expression of HIF-1α, which plays a key role in the regulation of genes such as VEGF and heme oxygenase 1 (55). The western blot analysis results of the present study suggested that CDK12 activates Akt and upregulates VEGFA expression, while IGFBP3 has the opposite effect of CDK12. Increased p-Akt and VEGFA levels were observed in siIGFBP3/sgCDK12 group cells relative to sgCDK12 group cells or a convergence of p-Akt and VEGFA content in siIGFBP3/sgCDK12 group cells to sgNT

group cells. Therefore, it was concluded that CDK12 inhibits IGFBP3 and thus activates Akt and upregulates VEGFA. Transplanted tumors were made into sections and stained for IHC: CDK12 expression was higher in sgNT group tissues than in the sgCDK12 group; IGFBP3 expression was lower than in sgCDK12 group; VEGF expression was higher than that in the sgCDK12 group and MVD was higher than that in the sgCDK12 group. The IHC results together with western blot analysis results supported the conclusion that CDK12 inhibits IGFBP3 expression and promotes angiogenesis in PCa. The results of the tube formation assay served as supporting evidence to confirm the hypothesis that CDK12 promotes PCa angiogenesis by inhibiting IGFBP3.

In addition to Akt and VEGF as aforementioned, the authors consider that androgen receptor (AR) is likely involved upstream/downstream of CDK12/IGFBP3 in mediating PCa progression, as AR is critical to PCa pathogenesis (56). The effect of CDK12/IGFBP3 on AR was not evaluated in the present study, which is one of the limitations of the present study. The authors will further explore the role of AR in this process in the future.

Given the stable knockdown of CDK12 by CRISPR/CAS9, transplanted tumor models were constructed in nude mice using PC3 cells from the sgNT and sgCDK12 groups. Mice were sacrificed when the largest transplanted tumor was nearly 15 mm in diameter, during which time it was observed that transplanted tumors from mice injected with sgNT group cells grew significantly faster than those from mice injected with sgCDK12 group cells. After removing the tumors, it was detected that the transplanted tumors of mice in the sgNT group were larger in size than those in the sgCDK12 group. It was thus demonstrated from *in vivo* experiments that CDK12 promotes the proliferation of PCa cells, which is consistent with the results of the previous *in vitro* experiments and those of Lei *et al* (35). As supplementary material, the relationship between CDK12, IGFBP3 and OS in PCa patients was analyzed separately after selecting the 'prostate adenocarcinoma' type in the LinkedOmics database. The results revealed that patients with higher CDK12 expression had a worse prognosis; those with higher IGFBP3 expression had an improved prognosis. However, the results were not statistically significant. Finally, the authors recognize that the limitations of the study include the lack of clinical human tissue samples as experiments on clinical specimens are critical.

Acknowledgements

The authors would like to especially thank the group of Professor Hu at Southern University of Science and Technology (Shenzhen, China) for sharing the results of RNA sequencing analysis as well as Dr Wang at the First Affiliated Hospital of Anhui Medical University (Hefei, China) for providing the cell lines.

Funding

The present study was supported by the National Natural Science Foundation of China (grant no. 81972414) and the Key Natural Science Research Project of Anhui Universities (grant no. 2023AH053332).

Availability of data and materials

All data generated or analyzed during this study are included in this published article. The datasets generated and/or analyzed during the current study are available in the Gene Expression Omnibus repository, (https://www.ncbi.nlm.nih.gov/geo/query/acc.cgi?acc=GSE246983).

Authors' contributions

YY and YC conceived the project and designed the study. KZ, WL, NL, XT, YL, SY, YH, LF and WM performed the experiments and analyzed the data. YY and KZ wrote the original draft of the paper, with contributions from all authors. All authors have read and approved the final version of the manuscript. KZ and WL confirm the authenticity of all the raw data.

Ethics approval and consent to participate

The animal study was approved by the Experimental Animal Ethics Committee of Anhui Medical University (approval no. LLSC20190458; Hefei, China).

Patient consent for publication

Not applicable.

Competing interests

The authors declare that they have no competing interests.

References

1. Daniyal M, Siddiqui ZA, Akram M, Asif HM, Sultana S and Khan A: Epidemiology, etiology, diagnosis and treatment of prostate cancer. Asian Pac J Cancer Prev 15: 9575-9578, 2014.
2. Rebbeck TR: Prostate cancer genetics: Variation by race, ethnicity, and geography. Semin Radiat Oncol 27: 3-10, 2017.
3. Wang G, Zhao D, Spring DJ and DePinho RA: Genetics and biology of prostate cancer. Genes Dev 32: 1105-1140, 2018.
4. Liang H, Liu Y, Guo J, Dou M, Zhang X, Hu L and Chen J: Progression in immunotherapy for advanced prostate cancer. Front Oncol 13: 1126752, 2023.
5. Siegel RL, Miller KD and Jemal A: Cancer statistics, 2018. CA Cancer J Clin 68: 7-30, 2018.
6. Lassi K and Dawson NA: Emerging therapies in castrate-resistant prostate cancer. Curr Opin Oncol 21: 260-265, 2009.
7. Wang W, Kong P, Feng K, Liu C, Gong X, Sun T, Duan X, Sang Y, Jiang Y, Li X, *et al*: Exosomal miR-222-3p contributes to castration-resistant prostate cancer by activating mTOR signaling. Cancer Sci 114: 4252-4269, 2023.
8. Netto GJ, Amin MB, Berney DM, Compérat EM, Gill AJ, Hartmann A, Menon S, Raspollini MR, Rubin MA, Srigley JR, *et al*: The 2022 World Health Organization classification of tumors of the urinary system and male genital Organs-Part B: Prostate and urinary tract tumors. Eur Urol 82: 469-482, 2022.
9. Wang Z, Wang T, Hong D, Dong B, Wang Y, Huang H, Zhang W, Lian B, Ji B, Shi H, *et al*: Single-cell transcriptional regulation and genetic evolution of neuroendocrine prostate cancer. iScience 25: 104576, 2022.
10. Carmeliet P: Angiogenesis in health and disease. Nat Med 9: 653-660, 2003.
11. Fabian KL and Storkus WJ: Immunotherapeutic targeting of tumor-associated blood vessels. Adv Exp Med Biol 1036: 191-211, 2017.
12. Lammert E and Axnick J: Vascular lumen formation. Cold Spring Harb Perspect Med 2: a006619, 2012.
13. Lui GYL, Grandori C and Kemp CJ: CDK12: An emerging therapeutic target for cancer. J Clin Pathol 71: 957-962, 2018.

14. Liu H, Liu K and Dong Z: Targeting CDK12 for cancer therapy: Function, mechanism, and drug discovery. Cancer Res 81: 18-26, 2021.
15. Liu B, Lee KW, Anzo M, Zhang B, Zi X, Tao Y, Shiry L, Pollak M, Lin S and Cohen P: Insulin-like growth factor-binding protein-3 inhibition of prostate cancer growth involves suppression of angiogenesis. Oncogene 26: 1811-1819, 2007.
16. Seligson DB, Yu H, Tze S, Said J, Pantuck AJ, Cohen P and Lee KW: IGFBP-3 nuclear localization predicts human prostate cancer recurrence. Horm Cancer 4: 12-23, 2013.
17. Johnson MA and Firth SM: IGFBP-3: A cell fate pivot in cancer and disease. Growth Horm IGF Res 24: 164-173, 2014.
18. Oh SH, Kim WY, Kim JH, Younes MN, El-Naggar AK, Myers JN, Kies M, Cohen P, Khuri F, Hong WK, *et al*: Identification of insulin-like growth factor binding protein-3 as a farnesyl transferase inhibitor SCH66336-induced negative regulator of angiogenesis in head and neck squamous cell carcinoma. Clin Cancer Res 12: 653-661, 2006.
19. Livak KJ and Schmittgen TD: Analysis of relative gene expression data using real-time quantitative PCR and the 2(-Delta Delta C(T)) method. Methods 25: 402-408, 2001.
20. Bai N, Xia F, Wang W, Lei Y, Bo J and Li X: CDK12 promotes papillary thyroid cancer progression through regulating the c-myc/β-catenin pathway. J Cancer 11: 4308-4315, 2020.
21. Shih HJ, Chen CL and Torng PL: IGFBP3 inhibits angiogenesis through intracellular regulation of THBS1 expression. Am J Cancer Res 10: 1728-1744, 2020.
22. He G, Li M, Fang L, Xu L, Huang X, Zheng L, Yang L, Luo W, Cai Y, Ma W, *et al*: N-Myc induces the tumor progression of prostate cancer by regulating FSCN1. Oncol Rep 44: 2265-2274, 2020.
23. Marciscano AE and Barbieri CE: CDK12 Gene alterations in prostate cancer: Present, but clinically actionable? Eur Urol 78: 680-681, 2020.
24. Liang S, Hu L, Wu Z, Chen Z, Liu S, Xu X and Qian A: CDK12: A potent target and biomarker for human cancer therapy. Cells 9: 1483, 2020.
25. Wu YM, Cieślik M, Lonigro RJ, Vats P, Reimers MA, Cao X, Ning Y, Wang L, Kunju LP, de Sarkar N, *et al*: Inactivation of CDK12 delineates a distinct immunogenic class of advanced prostate cancer. Cell 173: 1770-1782.e14, 2018.
26. Lotan TL and Antonarakis ES: CDK12 Deficiency and the immune microenvironment in prostate cancer. Clin Cancer Res 27: 380-382, 2021.
27. Dallinga MG, Habani YI, Kayser RP, Van Noorden CJF, Klaassen I and Schlingemann RO: IGF-binding proteins 3 and 4 are regulators of sprouting angiogenesis. Mol Biol Rep 47: 2561-2572, 2020.
28. Li CL, Liu B, Wang ZY, Xie F, Qiao W, Cheng J, Kuang JY, Wang Y, Zhang MX and Liu DS: Salvianolic acid B improves myocardial function in diabetic cardiomyopathy by suppressing IGFBP3. J Mol Cell Cardiol 139: 98-112, 2020.
29. Oh SH, Kim WY, Lee OH, Kang JH, Woo JK, Kim JH, Glisson B and Lee HY: Insulin-like growth factor binding protein-3 suppresses vascular endothelial growth factor expression and tumor angiogenesis in head and neck squamous cell carcinoma. Cancer Sci 103: 1259-1266, 2012.
30. Ranke MB: Insulin-like growth factor binding-protein-3 (IGFBP-3). Best Pract Res Clin Endocrinol Metab 29: 701-711, 2015.
31. Lin JS and Lai EM: Protein-protein interactions: Co-immunoprecipitation. Methods Mol Biol 1615: 211-219, 2017.
32. Antonarakis ES, Isaacsson Velho P, Fu W, Wang H, Agarwal N, Sacristan Santos V, Maughan BL, Pili R, Adra N, Sternberg CN, *et al*: CDK12-Altered prostate cancer: Clinical features and therapeutic outcomes to standard systemic therapies, poly (ADP-Ribose) polymerase inhibitors, and PD-1 inhibitors. JCO Precis Oncol 4: 370-381, 2020.
33. Wang X, Chen H, Luo J and Xie L: CDK12 mutation in advanced prostate cancer: A marker for clinical subtype? Eur Urol 77: 342-343, 2020.
34. Rescigno P, Gurel B, Pereira R, Crespo M, Rekowski J, Rediti M, Barrero M, Mateo J, Bianchini D, Messina C, *et al*: Characterizing CDK12-Mutated prostate cancers. Clin Cancer Res 27: 566-574, 2021.
35. Lei H, Wang Z, Jiang D, Liu F, Liu M, Lei X, Yang Y, He B, Yan M, Huang H, *et al*: CRISPR screening identifies CDK12 as a conservative vulnerability of prostate cancer. Cell Death Dis 12: 740, 2021.
36. Qin Z, Li X, Tang J, Jiang X, Yu Y, Wang C, Xu W, Hua Y, Yu B and Zhang W: Association between insulin-like growth factor-binding protein-3 polymorphism-202 A/C and the risk of prostate cancer: A meta-analysis. Onco Targets Ther 9: 5451-5459, 2016.
37. Beveridge DJ, Richardson KL, Epis MR, Brown RAM, Stuart LM, Woo AJ and Leedman PJ: The tumor suppressor miR-642a-5p targets Wilms Tumor 1 gene and cell-cycle progression in prostate cancer. Sci Rep 11: 18003, 2021.
38. Kim WY, Kim MJ, Moon H, Yuan P, Kim JS, Woo JK, Zhang G, Suh YA, Feng L, Behrens C, *et al*: Differential impacts of insulin-like growth factor-binding protein-3 (IGFBP-3) in epithelial IGF-induced lung cancer development. Endocrinology 152: 2164-2173, 2011.
39. Kim JH, Choi DS, Lee OH, Oh SH, Lippman SM and Lee HY: Antiangiogenic antitumor activities of IGFBP-3 are mediated by IGF-independent suppression of Erk1/2 activation and Egr-1-mediated transcriptional events. Blood 118: 2622-2631, 2011.
40. Oh SH, Whang YM, Min HY, Han SH, Kang JH, Song KH, Glisson BS, Kim YH and Lee HY: Histone deacetylase inhibitors enhance the apoptotic activity of insulin-like growth factor binding protein-3 by blocking PKC-induced IGFBP-3 degradation. Int J Cancer 131: 2253-2263, 2012.
41. Park K, Kim JH, Jeon HG, Byun SS and Lee E: Influence of IGFBP3 gene polymorphisms on IGFBP3 serum levels and the risk of prostate cancer in low-risk Korean men. Urology 75: 1516.e1-e7, 2010.
42. Dudley AC: Tumor endothelial cells. Cold Spring Harb Perspect Med 2: a006536, 2012.
43. Hess K, Spille DC, Adeli A, Sporns PB, Zitta K, Hummitzsch L, Pfarr J, Stummer W, Brokinkel B, Berndt R and Albrecht M: Occurrence of fibrotic tumor vessels in grade I meningiomas is strongly associated with vessel density, expression of VEGF, PlGF, IGFBP-3 and tumor recurrence. Cancers (Basel) 12: 3075, 2020.
44. Folkman J: Tumor angiogenesis. Adv Cancer Res 19: 331-358, 1974.
45. Farnsworth RH, Lackmann M, Achen MG and Stacker SA: Vascular remodeling in cancer. Oncogene 33: 3496-3505, 2014.
46. Chang KH, Chan-Ling T, McFarland EL, Afzal A, Pan H, Baxter LC, Shaw LC, Caballero S, Sengupta N, Li Calzi S, *et al*: IGF binding protein-3 regulates hematopoietic stem cell and endothelial precursor cell function during vascular development. Proc Natl Acad Sci USA 104: 10595-10600, 2007.
47. Zhao HJ, Klausen C, Zhu H, Chang HM, Li Y and Leung PCK: Bone morphogenetic protein 2 promotes human trophoblast cell invasion and endothelial-like tube formation through ID1-mediated upregulation of IGF binding protein-3. FASEB J 34: 3151-3164, 2020.
48. Granata R, Trovato L, Lupia E, Sala G, Settanni F, Camussi G, Ghidoni R and Ghigo E: Insulin-like growth factor binding protein-3 induces angiogenesis through IGF-I- and SphK1-dependent mechanisms. J Thromb Haemost 5: 835-845, 2007.
49. Lee HJ, Lee JS, Hwang SJ and Lee HY: Insulin-like growth factor binding protein-3 inhibits cell adhesion via suppression of integrin β4 expression. Oncotarget 6: 15150-15163, 2015.
50. Melincovici CS, Boşca AB, Şuşman S, Mărginean M, Mihu C, Istrate M, Moldovan IM, Roman AL and Mihu CM: Vascular endothelial growth factor (VEGF)-key factor in normal and pathological angiogenesis. Rom J Morphol Embryol 59: 455-467, 2018.
51. Shariati M and Meric-Bernstam F: Targeting AKT for cancer therapy. Expert Opin Investig Drugs 28: 977-988, 2019.
52. Revathidevi S and Munirajan AK: Akt in cancer: Mediator and more. Semin Cancer Biol 59: 80-91, 2019.
53. Luo Z, Fujio Y, Kureishi Y, Rudic RD, Daumerie G, Fulton D, Sessa WC and Walsh K: Acute modulation of endothelial Akt/PKB activity alters nitric oxide-dependent vasomotor activity in vivo. J Clin Invest 106: 493-499, 2000.
54. Dimmeler S, Fleming I, Fisslthaler B, Hermann C, Busse R and Zeiher AM: Activation of nitric oxide synthase in endothelial cells by Akt-dependent phosphorylation. Nature 399: 601-605, 1999.
55. Semenza GL: HIF-1 and tumor progression: Pathophysiology and therapeutics. Trends Mol Med 8 (4 Suppl): S62-S67, 2002.
56. Dai C, Heemers H and Sharifi N: Androgen signaling in prostate cancer. Cold Spring Harb Perspect Med 7: a030452, 2017.